Archives of Acoustics Online First August 21, 2025 https://doi.org/10.24425/aoa.2025.154821

Research Paper

Simulation and Experiment of a Medium-Distance Underwater Ultrasonic Wireless Power Transfer System

Chenyu LIAO[(1)], Huaiqing ZHANG[(2)*], Zhi LI[(1)], Qian ZHANG[(1)]

[(1)] *College of Electrical Engineering, Chongqing University*
Chongqing, China

[(2)] *Department of Electrical Engineering, Chongqing University*
Chongqing, China

*Corresponding Author e-mail: zhanghuaiqing@cqu.edu.cn

Received February 28, 2025; accepted July 4, 2025;
published online August 21, 2025.

This paper focuses on ultrasonic wireless power transfer (UWPT), a form of underwater wireless power transfer (WPT) using acoustic (ultrasonic) waves. We propose an ultrasonic transducer designed based on the Langevin transducer model, along with its equivalent circuit model for underwater transmission, tailored for efficient medium-distance underwater WPT. The performance of this transducer is simulated and analyzed using the acoustic-piezoelectric structure module in COMSOL. The results demonstrate that the transducer exhibits excellent underwater transmission characteristics. Additionally, an equivalent circuit model of the underwater UWPT system is developed and analyzed to characterize its transmission properties. For validation, a prototype UWPT is fabricated. At a 35 cm separation between the transmitter and receiver, the transmitter power is 2.5 W. With a 1.2 kΩ load, the received root mean square (RMS) voltage is measured at 22.8 V, corresponding to a received power of 433 mW and a transmission efficiency of 17 %. These results verify the proposed model, demonstrate a significant improvement in the transmission distance of underwater UWPT systems, and confirm the feasibility of medium-distance UWPT.

Keywords: underwater; wireless power transfer (WPT); ultrasonic; ultrasonic transducer.

1. Introduction

With the development of science and technology along with rising living standards, the global demand for electricity continues to grow, highlighting the limitations of traditional wireless power transmission (WPT) methods and increasing interest in WPT (Song *et al.*, 2021; Zhang *et al.*, 2019). WPT, which enables power transmission without physical contact, has demonstrated significant application potential through various methods such as magnetic resonance, inductive coupling, and far-field microwave power transfer (Roes *et al.*, 2013; Kim *et al.*, 2022; Singer, Robinson, 2021; Shin *et al.*, 2014; Sanni *et al.*, 2012; Valenta, Durgin, 2014). At present, electromagnetic wireless power transfer (EWPT) technologies are relatively mature. However, in underwater environment, the presence of electrolytes in seawater reduces the efficiency of EWPT, especially for long-distance transmission (Xu *et al.*, 2015). In the case of inductive coupling, the maximum operating distance is typically limited to only a few centimeters. In contrast, ultrasonic waves offer excellent transmission performance underwater, as sound waves undergo low attenuation in aqueous environments. Compared to electromagnetic waves, sound waves can propagate over long distances in water with lower energy loss. Therefore, ultrasonic wireless power transfer (UWPT) holds significant promise as an alternative to electromagnetic induction for underwater power delivery systems (Guida *et al.*, 2022).

Current research in UWPT technology has mostly focused on power transmission through metal walls and for subcutaneous medic. For instance, Toshihiko Ishiyama presented the concept of wireless charging for mobile electronic devices using ultrasonic trans-

ducer in air, transmitting 0.8 W of power over a distance of 0.3 m (Roes *et al.*, 2011). Bao *et al.* (2008) developed a kilowatt-scale high-power device that penetrated a metal wall at a frequency of 24.5 kHz to achieve 1 kW of UWPT through a metal wall. Chen *et al.* (2018) demonstrated underwater UWPT with a transmission efficiency of 31 % at a distance of 5 cm between the transmitter and receiver for transducer charging. Basaeri *et al.* (2019) employed piezoelectric ceramics to power an implantable medical device, delivering 0.7 mW of power to the receiving transducer over a distance of 20 mm.

In previous underwater UWPT systems, the transmission distance has typically been confined to short ranges (less than 10 cm). In this work, by employing 28 kHz ultrasonic transducers, we extend the transfer distance to 35 cm – placing it within the medium-range regime (10 cm–50 cm). We develop a Langevin-type transducer and employ COMSOL Multiphysics to simulate its underwater propagation characteristics. Additionally, we propose an equivalent circuit model of the underwater UWPT system and derive its theoretical transfer characteristics. The accuracy of the theoretical model and the performance of the underwater WPT system are further validated through experimental testing. The feasibility of mid-range UWPT is effectively demonstrated, which is of great significance for underwater wireless power delivery.

2. Underwater WPT system

The initial step in developing an UWPT system involves constructing the underwater WPT setup. The system comprises a signal source, ultrasonic transducers at both the transmitting and receiving ends, and an impedance matching circuit designed to optimize the receiving impedance. Since piezoelectric transducers operate most efficiently at their resonant frequency, a high-frequency signal generator supplies the transmitting ultrasonic transducer with a high-frequency signal at its resonant frequency of f_0 to generate ultrasonic waves. These waves propagate through the water and are received by the ultrasonic transducer at the receiving end, where they are converted back into electrical signals. Due to the capacitive nature of the ultrasonic transducer, an impedance matching circuit is employed to eliminate reactive power generated by the transducer and ensure maximum power transfer efficiency. The received signal is then rectified and filtered through a circuit to supply power for downstream electronic components. The structure of the underwater UWPT system is shown in Fig. 1.

The underwater ultrasonic transducer discussed in this paper is based on a Langevin-type design. It consists of a backing layer, piezoelectric ceramic elements, and a front matching layer. The Langevin transducer is constructed by stacking piezoelectric elements, which are compressed and held together in place by bolts positioned between the backing and the metal matching layer. This compression bolt applies a preload to the piezoelectric elements, maintaining them in a compressed state to prevent material fractures during high-power operation (Bao *et al.*, 2008).

From an acoustic perspective, the impedance mismatch between solid and liquid necessitates the inclusion of a matching layer to enhance transmission efficiency. The acoustic impedance of the metal at the front of the transducer is approximately 17.3 MRayl, while that of water is around 1.48 MRayl. When there is a significant mismatch in acoustic impedance between two materials, most of the sound waves will be reflected at the boundary, resulting in minimal transmission through the interface. Conversely, when the difference in acoustic impedance is relatively small, most of the sound waves can pass through the boundary. To ensure efficient underwater operation and achieve optimal acoustic impedance matching with water, a two-layer matching structure is required. One of these layers is composed of epoxy resin adhesive (Callens *et al.*, 2004).

The design principle is shown in Fig. 2. This method uses the classical transfer matrix method, where the thickness of each matching layer is T_n, and an acoustic impedance of the matching layer is Z_n. The transfer matrix of the n-th matching layer can be obtained as (Callens *et al.*, 2004):

$$T_n = \begin{bmatrix} \cos\theta_n & jZ_n \sin\theta_n \\ \dfrac{j}{Z_n}\sin\theta_n & \cos\theta_n \end{bmatrix}, \tag{1}$$

where λ_n is the wavelength of the n-th layer, t_n is the thickness of the n-th layer, $n = 1, 2, 3, 4$, and the phase shift $\theta_n = \frac{2\pi t_n}{\lambda_n}$.

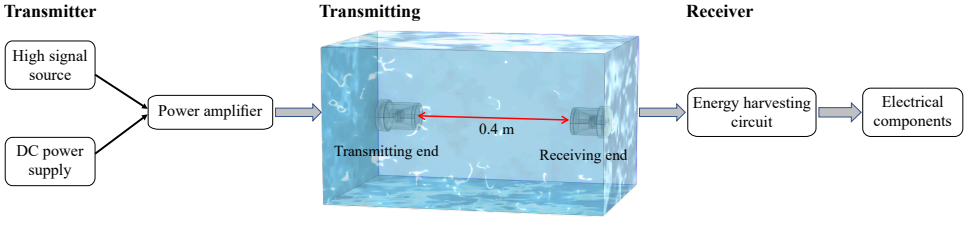

Fig. 1. Underwater UWPT system.

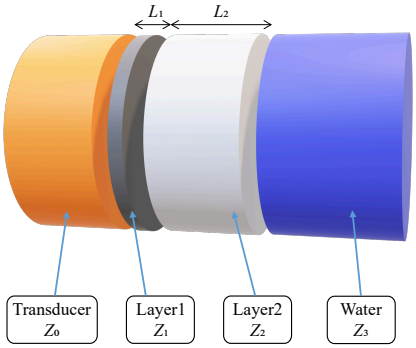

Fig. 2. Schematic diagram of the multi-layer matching transducer.

Impedance matching is achieved by adjusting the equivalent impedance of the ultrasonic transducer $Z_{eq} = Z_3$ at the transducer-dielectric boundary (Z_0 is the impedance of the transmission medium), where Z_{eq} is

$$Z_{eq} = \frac{T_{11}Z_0 + T_{12}}{T_{21}Z_0 + T_{22}}, \tag{2}$$

where T_{ij} is an element of the multilayer matching structure transfer matrix $\mathbf{T}$, defined by

$$T_{eq} = T_1T_2T_3T_4 = \begin{bmatrix} T_{11} & T_{12} \\ T_{21} & T_{22} \end{bmatrix}. \tag{3}$$

The primary advantage of this method lies in its ability to broaden the range of materials suitable for acoustic impedance matching, thereby enhancing the efficiency of underwater ultrasonic power transmission. The transducer was designed to operate at a frequency of 28 kHz, with the thickness of each layer calculated using the relevant formula: 0.3 cm for the epoxy adhesive layer and 0.98 cm for the plexiglass layer. Using these parameters, the ultrasonic transducer was modeled in COMSOL Multiphysics, as shown in Fig. 3.

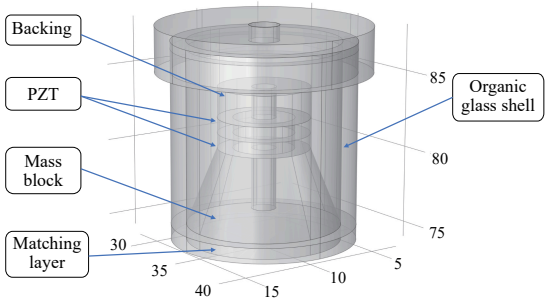

Fig. 3. Transducer simulation model.

The interior of the transducer housing is airtight. Since the acoustic impedance of air is 4×10^{-4} MRayl (Selfridge, 1985), which differs significantly from both the piezoelectric ceramic and the metal acoustic impedance at the front end, the ultrasonic waves encounter a solid-gas boundary inside the housing.

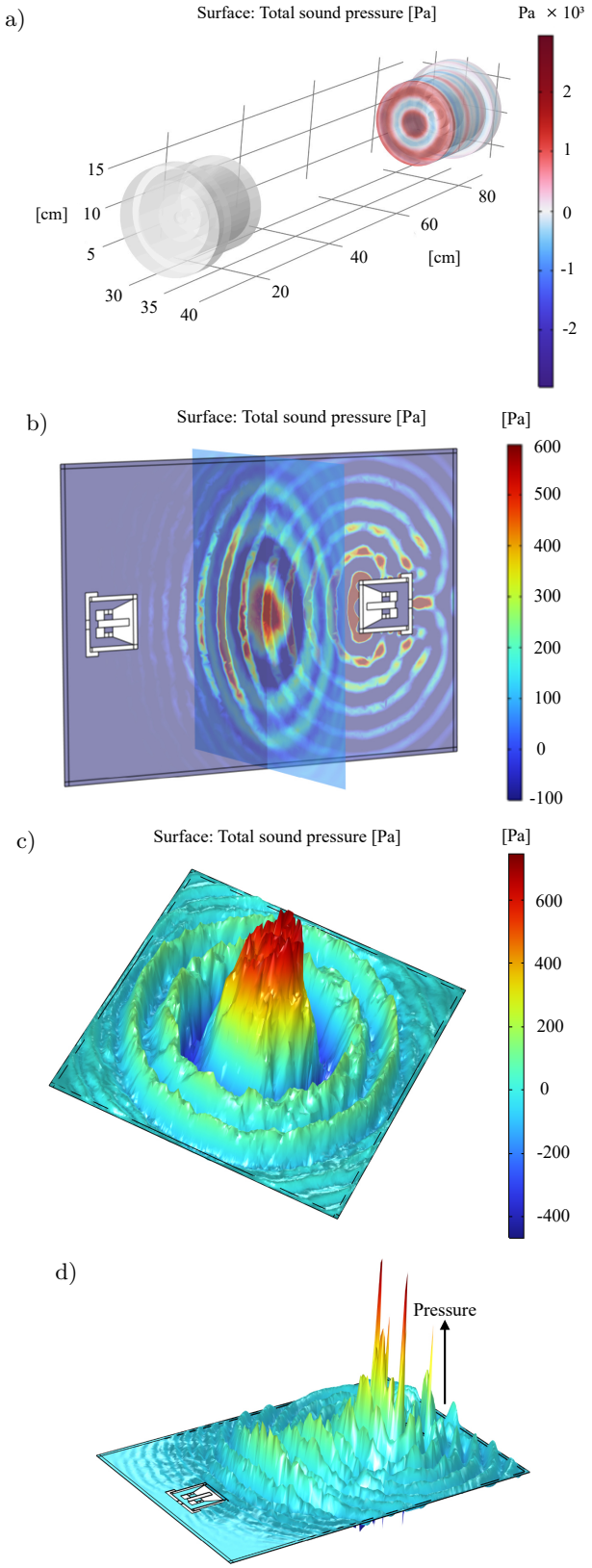

Fig. 4. COMSOL simulation of transducer sound pressure: a) sound pressure distribution at the front face of the transducer; b) multi-slice sound pressure maps; c) sound pressure levels at 25 cm from the transducer; d) YZ-plane acoustic pressure distribution map from the COMSOL simulation.

This design effectively minimizes the side lobes of the ultrasonic transducer, thereby ensuring efficient ultrasound emission from the front face.

After that, COMSOL Multiphysics was used to simulate the underwater performance of the ultrasonic transducer. The simulation results reveal that when the transducer operates underwater, the sound field energy generated by the transducer is primarily concentrated at its front face, as shown in Fig. 4a. By constructing an underwater multi-plane acoustic pressure map, as shown in Fig. 4b, it is observed that the side lobe pressure levels of the transducer are minimal, while a pressure level at the center of the transmission is significantly high. This indicates the transducer's excellent transmission characteristics. Furthermore, measurements of the sound pressure level at a distance of 25 cm from the transducer confirm that the central sound pressure is the strongest, as shown in Fig. 4c. The effective underwater transmission characteristics of the transducer can be seen in the YZ-plane, as shown in Fig. 4d.

3. System modeling and experimentation

3.1. Equivalent circuit of ultrasonic transducer

In order to increase the power of the transducer and the received efficiency, proper impedance matching is essential. Therefore, establishing an equivalent circuit model of the ultrasonic transducer has to be established first. Based on the operating principles of the transducer, its equivalent circuit model near the resonant frequency is shown in Fig. 5 (Fai *et al.*, 2015).

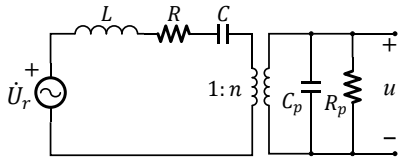

Fig. 5. Equivalent circuit diagram of ultrasonic transducer.

In Fig. 5, $\dot{U}_r$ is the induced voltage, C_p is the intrinsic capacitance of the piezoelectric material, and R_p is the leakage resistance associated with C_p. Additionally, L represents the transducer's mass, C denotes the stiffness, and R corresponds to the mechanical damping. Figure 6 illustrates the equivalent circuit diagram of the underwater UWPT system. When the excitation frequency applied to the transmitting transducer face matches it resonant frequency f_0, the transmitting transducer generates maximum mechanical vibration, given by

$$f_0 = \frac{1}{2\pi\sqrt{L_0 C_0}}. \tag{4}$$

The transducer at the receiving end converts the incoming ultrasonic signal into an electrical signal. At this point, the input voltage at the receiving end can be modeled as a controlled current voltage source (CCVS), with a magnitude of $k\dot{I}$, where k is the control coefficient. The control coefficient k represents the attenuation coefficient of ultrasonic waves propagating in water. Under fixed experimental conditions and a predetermined propagation distance, the ultrasonic wave traveling from the transmitter to the receiver undergoes attenuation characterized by this constant coefficient k, which quantifies the energy loss incurred within the medium. In the equivalent electrical circuit, this acoustic attenuation is modeled by a CCVS that delivers the attenuated signal at the receiver. Consequently, a larger value of k corresponds to lower acoustic attenuation.

The parameters L_0, R_0, C_0 and L_1, R_1, C_1 are derived from the LRC impedance shown in Fig. 5. C_{p0} and C_{p1} represent the intrinsic capacitance of the piezoelectric transducer, while R_{p1} denotes the equivalent resistance of the energy radiated by the transducer. Furthermore, L_b represents the back-end impedance matching inductance, and R_b denotes the impedance matching resistance.

Next, we calculate the equivalent input resistance Z_1 seen from terminals a and b. When $\dot{U}_r = 0$, the equivalent impedance as viewed from the right end is Z_1, and the equivalent output impedance of the ultrasonic transducer at its receiving end is calculated as

$$Z_1 = Z_{p1} // Z_2 = \frac{Z_1 Z_2}{Z_1 + Z_2}. \tag{5}$$

When the transducer operates at its resonant frequency f_0, L_1 resonates in series with C_1. At this point, the equivalent impedance Z_1 is given by

$$Z_1 = \frac{R_1}{(R_1\omega C_{p1})^2 + 1} - j\frac{R_1^2\omega C_{p1}}{(R_1\omega C_{p1})^2 + 1}. \tag{6}$$

To eliminate the reactive power, the imaginary component of the impedance Z must be set to zero. Consequently, an external inductance L_b is

$$L_b = \frac{R_1^2 C_{p1}}{(R_1\omega C_{p1})^2 + 1}. \tag{7}$$

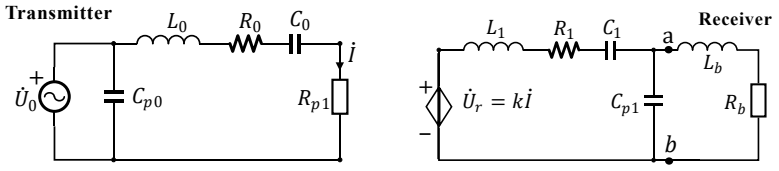

Fig. 6. Equivalent circuit of an underwater UWPT system.

After compensation, the equivalent output impedance is

$$Z_2 = \frac{R_1}{(R_1\omega C_{p1})^2 + 1}. \tag{8}$$

The simplified equivalent circuit diagram after impedance matching is shown in Fig. 7.

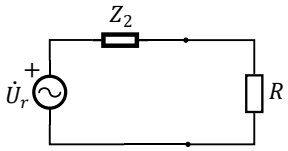

Fig. 7. Simplified circuit modeling.

The voltage across R can be calculated as U_1, and according to the maximum power transfer theorem, the power at the receiving end is

$$U_1 = \frac{R\dot{U}_r}{R + Z_2}, \tag{9}$$

$$P_1 = \frac{\dot{U}_r^2}{4Z_2}, \tag{10}$$

where P_1 is the maximum accepted power obtained when $R = Z_2$ according to the maximum power theory.

To obtain the impedance of the ultrasonic transducer, an impedance analyzer (Agilent 4294A) is used to measure the impedance of the ultrasonic transducer. Its internal impedance is shown in Fig. 8, indicating that its impedance reaches a minimum at 26.9 kHz, corresponding to its resonant frequency, with an equivalent resistance of 1200 Ω.

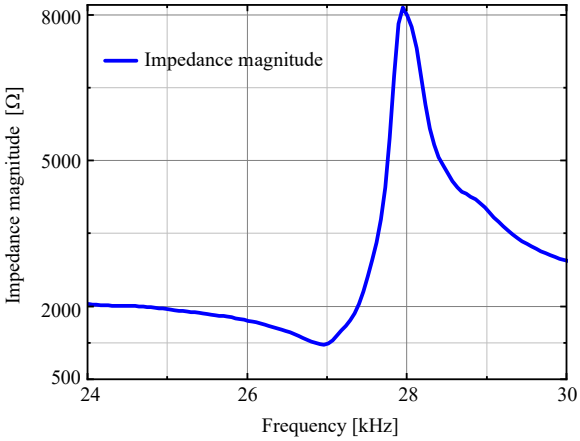

Fig. 8. Ultrasonic transducer impedance amplitude vs. frequency.

3.2. Underwater ultrasonic power transfer experiment

The underwater ultrasonic transducer used in this experiment is based on a Langevin structural design machined by the manufacturer. The receiver is identical in size to the transmitter, with a circular vibrating surface measuring 80 mm in diameter and a resonant frequency of 28 kHz. The actual resonant frequency was measured to be 26.9 kHz using an impedance analyzer. By substituting $C_{p1} = 2$ nF and $R = 1.5$ kΩ into Eqs. (7) and (8), the equivalent impedance is calculated to be approximately 1200 Ω, and the matching inductance is 3.58 mH.

A high-frequency AC signal, matching the resonant frequency of the transducer, is generated by a high-frequency signal source. After amplification by a power amplifier, a voltage of 40 V is applied at the transmitting end. The assembled underwater UWPT system is shown in Fig. 9.

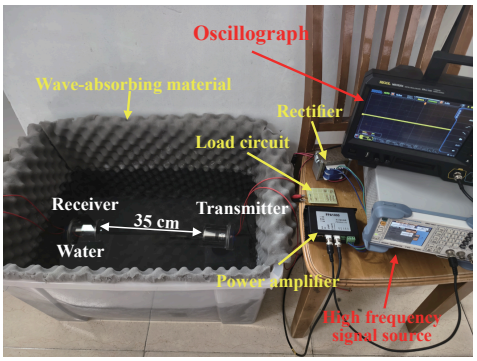

Fig. 9. Underwater UWPT system.

Piezoelectric components in ultrasonic transducers operate exclusively at their inherent resonant frequency, where they achieve maximum amplitude and optimal power conversion efficiency. When the signal frequency supplied to the ultrasonic transducer deviates from this resonant frequency, both the ultrasonic power generated at the transmitting end and the acoustic-to-electric conversion efficiency at the receiving end decrease significantly. This also causes a marked reduction in the received voltage at the receiving end. Moreover, when the receiving ultrasonic transducer is laterally displaced from the transmitting transducer (i.e., off the transmitter's central axis), the received power decreases significantly – falling by 40 % at a 5 cm offset. This indicates that the acoustic power generated by the transmitter is predominantly concentrated in the central region. These observations are consistent with the COMSOL simulation results.

As shown in Fig. 10, the maximum voltage at the receiving end occurs when the signal source output frequency is 26.88 kHz, with a peak-to-peak value reaching 64 V. Notably, this resonant frequency is slightly lower than previously measured values. This reduction in resonance frequency is attributed to the addition of matching layers onto the exterior of the Langevin transducer (Fei *et al.*, 2015).

Resistors of varying sizes are used as loads at the receiving end of the ultrasonic transducer to examine how the load power changes with different resis-

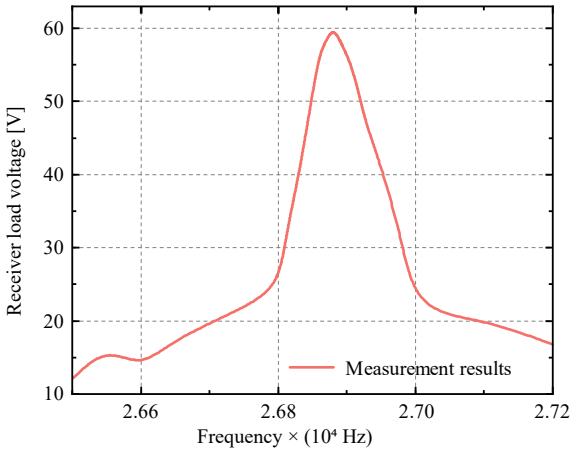

Fig. 10. Load acceptance voltage vs. input signal frequency.

tance values. While the theoretical model closely predicts the output characteristics, slight deviations from the experimental data are observed, likely due to conductance variations induced by changes in load resistance. As shown in Fig. 11, the load power increases with rising resistance, reaching an RMS voltage of 22.8 V across the load at an impedance of 1.2 kΩ, resulting in a real power output of 433 mW. However, when the resistance deviates from this optimal value, the load power decreases significantly.

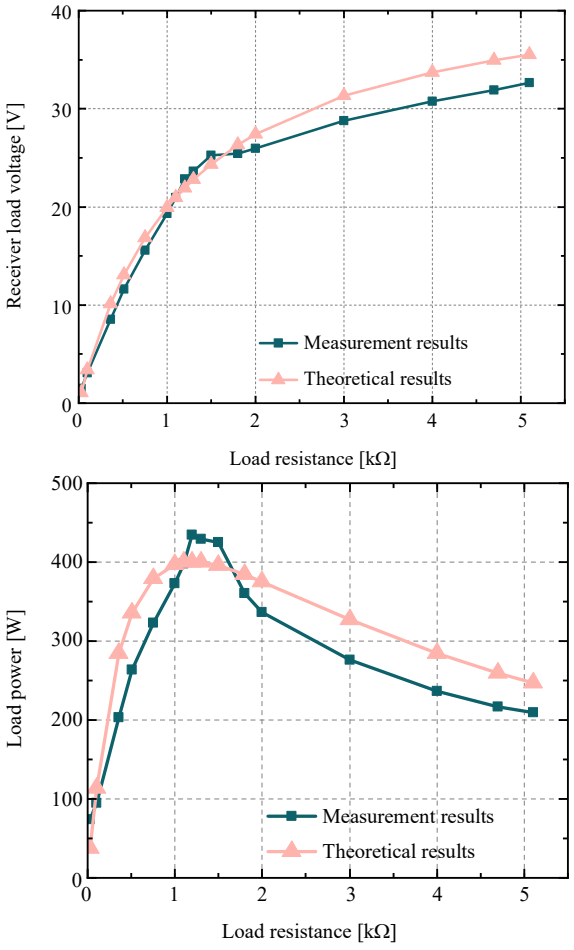

Fig. 11. Output performance characteristics for different resistive loads.

When the transmitter delivers a real power of 2.5 W, the system achieves an effective transmission efficiency of 17 % over a 35 cm distance, corresponding to a received power of 433 mW. This study demonstrates the feasibility of medium-distance underwater UWPT, offering a viable solution to the challenges associated with underwater ultrasonic power transmission.

4. Conclusion

In this paper, we proposed an ultrasonic transducer designed based on the Langevin transducer model, along with its equivalent circuit model for underwater UWPT systems. The performance of the transducer was simulated and analyzed using the acoustic-piezoelectric structure module in COMSOL. The results demonstrated that the ultrasonic transducer exhibits excellent underwater transmission characteristics. Subsequently, the equivalent circuit model was employed to theoretically predict the transmission characteristics of the UWPT system. The model provided an effective means of calculating the expected performance of the designed system. An experimental platform for the underwater UWPT system was developed to validate the proposed model. The measured efficiency matched the theoretical predictions within experimental error.

Currently, UWPT distances are typically limited to millimeters or a few centimeters. The underwater ultrasonic transducer developed in this study significantly extends the transmission range, enabling WPT over a distance of 35 cm. The maximum transmission power of the UWPT system was calculated using the equivalent circuit model. Finally, the receiver registered a power output of 433 mW, corresponding to a net transmission efficiency of 17 %. It was demonstrated that the theoretical model aligns with the experimental data and effectively enhances both the transmission distance and efficiency of underwater WPT. This approach provides a non-contact solution for underwater wireless charging, enabling marine monitoring sensors and small autonomous underwater vehicles to recharge without frequent retrieval or cumbersome tethered connections. It may offer valuable benefits for future underwater sensor networks and small-scale autonomous subsea vehicles.

Future work will focus on constructing a larger water tank to enable ultrasonic energy transmission into the far-field region, thereby significantly extending the underwater WPT distance. Additionally, underwater phased-array techniques will be investigated to enable precise acoustic beam focusing and enhanced directivity, further improving transmission power.

Fundings

This research did not receive any specific grant from funding agencies in the public, commercial, or not-for-profit sectors.

Conflict of interest

The authors declare that they have no known competing financial interests or personal relationships that could have appeared to influence the work reported in this paper.

Authors' contribution

Chenyu Liao: conceptualization, methodology, formal analysis, software, visualization, validation, experimental execution, writing – original draft, review, and editing. Huaiqing Zhang: supervision, resources. Zhi Li: Guidance on the paper, writing – review and editing. Qian Zhang: Data collection, experimental execution. All authors reviewed and approved the final manuscript.

References

1. Bao X. *et al.* (2008), High-power piezoelectric acoustic-electric power feedthru for metal walls, [in:] *Proc. SPIE 6930, Industrial and Commercial Applications of Smart Structures Technologies 2008*, https://doi.org/10.1117/12.776473.
2. Basaeri H., Yu Y., Young D., Roundy S. (2019), A MEMS-scale ultrasonic power receiver for biomedical implants, *IEEE Sensors Letters*, **3**(4): 2501104, https://doi.org/10.1109/lsens.2019.2904194.
3. Callens D., Bruneel C., Assaad J. (2004), Matching ultrasonic transducer using two matching layers where one of them is glue, *NDT & E International*, **37**(8): 591–596, https://doi.org/10.1016/j.ndteint.2004.03.005.
4. Chen X., Xu K., Mou X., Li G. (2018), Comparison of inductively coupled and ultrasonically coupled wireless energy transmission technologies in seawater [in Chinese], *Journal of Electrical Machines and Control*, **22**(03): 9–16, https://doi.org/10.15938/j.emc.2018.03.002.
5. Fai L.H., Dai X., Hu A. (2015), Electrical modeling of a wireless ultrasonic power transfer system [in Chinese], *Chinese Journal of Electrical Engineering*, **30**(19): 85–89, https://doi.org/10.19595/j.cnki.1000-6753.tces.2015.19.012.
6. Fei C.L. *et al.* (2015), Design of matching layers for high-frequency ultrasonic transducers, *Applied Physics Letters*, **107**(12): 123505, https://doi.org/10.1063/1.4931703.
7. Guida R., Demirors E., Dave N., Melodia T. (2022), Underwater ultrasonic wireless power transfer: A battery-less platform for the Internet of Underwater Things, *IEEE Transactions on Mobile Computing*, **21**(5): 1861–1873, https://doi.org/10.1109/tmc.2020.3029679.
8. Kim H.S. *et al.* (2022), Ferroelectrically augmented contact electrification enables efficient acoustic energy transfer through liquid and solid media, *Energy & Environmental Science*, **15**(3): 1243–1255, https://doi.org/10.1039/d1ee02623b.
9. Roes M.G.L., Duarte J.L., Hendrix M.A.M., Lomonova E.A. (2013), Acoustic energy transfer: A review, *IEEE Transactions on Industrial Electronics*, **60**(1): 242–248, https://doi.org/10.1109/tie.2012.2202362.
10. Roes M.G.L., Hendrix M.A.M., Duarte J.L. (2011), Contactless energy transfer through air by means of ultrasound, [in:] *IECON 2011 – 37th Annual Conference of the IEEE Industrial Electronics Society*, pp. 1238–1243, https://doi.org/10.1109/IECON.2011.6119486.
11. Sanni A., Vilches A., Toumazou C. (2012), Inductive and ultrasonic multi-tier interface for low-power, deeply implantable medical devices, *IEEE Transactions on Biomedical Circuits and Systems*, **6**(4): 297–308, https://doi.org/10.1109/tbcas.2011.2175390.
12. Selfridge A.R. (1985), Approximate material properties in isotropic materials, *IEEE Transactions on Sonics and Ultrasonics*, **32**(3): 381–394, https://doi.org/10.1109/t-su.1985.31608.
13. Shin J. *et al.* (2014), Design and implementation of shaped magnetic-resonance-based wireless power transfer system for roadway-powered moving electric vehicles, *IEEE Transactions on Industrial Electronics*, **61**(3): 1179–1192, https://doi.org/10.1109/tie.2013.2258294.
14. Singer A., Robinson J.T. (2021), Wireless power delivery techniques for miniature implantable bioelectronics, *Advanced Healthcare Materials*, **10**(17): 2100664, https://doi.org/10.1002/adhm.202100664.
15. Song M. *et al.* (2021), Wireless power transfer based on novel physical concepts, *Nature Electronics*, **4**(10): 707–716, https://doi.org/10.1038/s41928-021-00658-x.
16. Valenta C.R., Durgin G.D. (2014), Harvesting wireless power: Survey of energy-harvester conversion efficiency in far-field, wireless power transfer systems, *IEEE Microwave Magazine*, **15**(4): 108–120, https://doi.org/10.1109/mmm.2014.2309499.
17. Xu K., Chen X., Liu D. (2015), Electrical impedance transformation technique for undersea ultrasonic coupled wireless energy transmission system [in Chinese], *Chinese Journal of Electrical Engineering*, **35**(17): 4461–4467, https://doi.org/10.13334/j.0258-8013.pcsee.2015.17.022.
18. Zhang Z., Pang H., Georgiadis A., Cecati C. (2019), Wireless power transfer – An overview, *IEEE Transactions on Industrial Electronics*, **66**(2): 1044–1058, https://doi.org/10.1109/tie.2018.2835378.